Fracture evolution in concrete compressive fatigue experiments based on X-ray micro-CT images

Ł. Skarżyński, I. Marzec and J. Tejchman

Faculty of Civil and Environmental Engineering

Gdańsk University of Technology, Poland

lskarzyn@pg.edu.pl, irek@pg.edu.pl, tejchmk@pg.edu.pl

Abstract

This study examines the fatigue performance of plain concrete specimens under uniaxial compression. The experimental program was developed for investigating the fracture evolution in concrete cubic specimens subjected to cyclic compression using the advanced X-ray micro-computed tomography system SkyScan 1173. As compared to other experiments, the 3D micro-CT damage images were shown for a various number of loading cycles. The quantitative evolution of the cracking volume with increasing damage revealed a strongly non-linear shape. The increase of the total crack volume was higher by 30% as compared to the monotonic fatigue test.

Keywords: micro-CT; plain concrete; compression; fatigue; fracture; meso-structure

1. Introduction

Fatigue is a process of progressive and permanent structural damage in materials which are subjected to repeatedly applied stresses and strains. As a result, macro-cracks or complete fracture occur after a certain number of repeated loading. The knowledge on the concrete behaviour in fatigue is essential for describing the behaviour of different engineering structures under repeated loads with random and varying amplitudes (e.g. concrete bridge desks, highway pavements, railway slab tracks, crane beams, wind power tower bases). The concrete fatigue is still a challenging topic in research works. In particular, the knowledge on the effect of cyclic loading on the evolution of fracture (crack initiation and growth, crack pattern, crack shape, crack number etc.) is still very limited in spite of many laboratory tests (e.g. [1-10]). This problem is also difficult since fatigue displacements and strains are subjected to a pronounced statistical scatter [11]. The progressive decreasing of the compression strength of concrete under cyclic loads happens due to internal damage. The fatigue test results on concrete in compression (mainly low and medium-cycle results) are usually described with the aid of the so-called Wöhler-curve or S-N curve ([2], [12-16]), that shows a linear relationship between the logarithm of the cycles' number

and maximum fraction of the monotonic compressive strength. There exist several factors that affect concrete fatigue behaviour. The fatigue strength mainly depends on the maximum and minimum stress in the cycle (often identified as the live load and dead load). An increase of the minimum stress and a decrease of the maximum stress level result in the increased fatigue strength for a given number of cycles. The frequency between 1 and 15 Hz has a little effect on the fatigue strength provided that the maximum stress is lower than about 75% of the monotonic strength. At higher stresses, the fatigue strength decreases with decreasing frequency ([16, 17]). The fatigue strength is also affected by water-cement ratio, cement content, amount of entrained air, concrete class, rest periods, curing conditions and age during loading [13]. It is assumed that damage linearly increases with the number of cycles applied at a certain stress level [17]. The strain at the concrete failure during fatigue tests corresponds to that at the peak load during quasi-static tests [18]. The failure meso-mechanism in concrete in fatigue compressive tests is almost the same as in monotonic compressive tests [19].

The presented research work is experimentally oriented. It is aimed at quantitative investigations of a three-dimensional (3D) crack evolution in plain concrete under uniaxial fatigue compression loading with very advanced non-destructive X-ray micro-computed tomography system SkyScan 1173 [20]. Micro-computed tomography (in short 'micro-CT') is a 3D imaging technique that uses X-rays to see the interior of different materials [21]. The micro-CT device performs 2D planar X-ray images and reconstructs the data into 2D cross-sectional slices that are further processed to obtain a full 3D image. Thus the volumetric information about changes in the internal micro/meso-structure may be achieved. In the paper, attention was focused on changes in the fracture volume with an increasing number of loading cycles in concrete compressive fatigue experiments. This knowledge is important to better understand a fracture process for enhancing the fatigue life of concrete members and structures. Our tomography system SkyScan 1173 was already successfully used for observations of a 3D fracture process inside concrete during different quasi-static monotonic tests: bending [22], uniaxial compression [23], tension splitting [24] and wedge splitting [25]. The micro-CT images of the concrete structure allowed us next for developing a very effective numerical 3D four-phase concrete model (composed of aggregate, cement matrix, macro-pores and interfacial transitional zones (ITZs)) within the discrete mechanics [23, 24, 26, 27] and continuum mechanics [22, 28, 29] to realistically reproduce strength, brittleness and fracture in plain concrete in different tests.

The novel elements of the current paper on concrete fatigue in compression are: 1) the full 3D damage maps with high-resolution of fractured concrete specimens for the different number of loading cycles in fatigue compression by considering concrete meso-structure (aggregate, cement matrix and pores) and 2) the quantitative estimation of changes of the cracks' and pores' volume (based on 3D damage maps)

70 with increasing cycle number and damage. Our experimental results may create a solid comparative

71 basis for numerical calculations using different fatigue continuum models for concrete based on

72 fracture/damage mechanics (e.g. [30-34]) or discrete mechanics ([35]). The micro-CT studies were also

73 carried out for steel fiber-reinforced concrete under low cycle fatigue in uniaxial compression by Vicente

74 et al. [19] that indicated a similar crack pattern in specimens under monotonic and cyclic loads. However,

75 the 2D images of concrete specimens were shown only and the micro-CT scans were solely made at the

76 beginning and end of tests. The micro-CT technique was also used in fatigue loading tests for scanning

77 of other engineering materials ([36, 37]). To our knowledge, 3D micro-CT scans of concrete specimens

78 at different loading cycles in fatigue compression have not been performed yet.

79

2. Specimen preparation, experimental set-up and distribution of pores

81

Specimen preparation

83 The laboratory fatigue experiments on concrete in uniaxial compression were carried out at the Gdansk

84 University of Technology. The concrete specimens were composed of an ordinary Portland cement

85 (CEM I 32.5 R), sand and gravel particles and water. The round-shape sand and gravel particles were

86 used with the maximum diameter of d_{max}=16 mm, mean diameter of d_{50}=2 mm and particle volume of

87 β=75% (Figure 1). The water/cement ratio was fixed to 0.42. The composition of the concrete mix was

88 described in Table 1. A small super plasticizer quantity was used to improve the workability of the fresh

89 concrete. The tests were carried out on relatively small concrete cubes of 40×40×40 mm^3 to obtain a

90 very high resolution of 3D micro-CT images of fractured concrete specimens. The cubes were cut out

91 from the same concrete block of the size 500×500×200 mm^3 after the seventh day. The concrete block

92 was covered with a plastic sheet during the initial curing period to avoid the surface evaporation and

93 autogenous shrinkage. They were next kept for 28 days in water. The uniaxial compressive strength f_c

94 was measured on three cube concrete specimens 10×10×10 cm^3 and Young's modulus E and Poisson's

95 ratio υ were determined on three cylindrical concrete specimens 15×30 cm^2. The mean measured values

96 were: f_c=51.81 MPa with the standard deviation of 3.36 MPa, E=36.1 GPa with the standard deviation

97 of 2.29 GPa and υ=0.22 with the standard deviation of 0.03. The mean tensile strength during three-point

98 bending on three concrete specimens 4×4×16 cm^2 was 4.04 MPa. The monotonic and fatigue tests were

99 conducted using the servo-hydraulic machine Zwick Roell HB250 (Figure 2) with the maximum loading

0 capacity of 250 kN and maximum frequency of 15 Hz. The machine was equipped with two compressive

1 steel plates and the cubes were always loaded along the casting direction (vertical axis). A sinusoidal

2 vertical force was applied along the top boundary in fatigue tests. The vertical force F and the axial

3 displacement u were continuously monitored and recorded. Initially, a monotonic test was carried out

4 with the controlled vertical displacement rate of 0.002 mm/min. The mean maximum vertical force was

3

105   F_{max}=81 kN that results in the uniaxial compressive strength of f_c=51.5 MPa which was almost equal to

106   the experimental results for the concrete specimens of 100×100×100 mm^3. Thus the size effect on the

107   nominal strength was negligible in the tests. However, the size effect on the concrete brittleness existed,

108   i.e. the ductility was larger for smaller specimens. Next, three cyclic tests were performed on cubic

109   concrete specimens during which the fatigue test parameters were as follows: the maximum stress

110   σ_{max}=38.5 MPa and minimum stress σ_{min}=19 MPa with the stress level $S_{\max} = \sigma_{max}/f_c = 0.75$ and

111   $S_{\min} = \sigma_{min}/f_c = 0.37$, and stress ratio $R = \sigma_{min}/\sigma_{max}$=0.5. The frequency of cyclic loading tests

112   with the constant amplitude was always f=2 Hz. The assumed value of S was rational from the point of

113   the design of concrete members in order to avoid the frequency effect. The frequency variations between

114   1 and 15 Hz have, namely, an insignificant effect on the fatigue strength provided that the maximum

115   stress level is smaller than 75% of the monotonic static strength ([16, 17]). The expected fatigue life of

116   concrete specimens was about N=60,000 cycles according to Model Code 2010 [14] ($\log N =$

117   $(12 + 16S_{\min} + 8S_{\min}^2)(1 - S_{\max})$). Although the number of concrete specimens was low (3), the

118   calculated fatigue experimental results were similar with respect to the number of loading cycles leading

119   specimens to the failure, changes of cracks' and pores' volumes and cracks' distributions.

120

121   **Experimental set-up**

122   The cracking evolution in concrete during fatigue cyclic tests was investigated using the advanced

123   X-ray micro-computed tomography system SkyScan 1173 (Figure 3). This system represents the newest

124   generation in high-resolution desktop X-ray micro-tomography technologies for 3D scanning [20]. The

125   technology defines the density of each specimen voxel by assigning different shades of grey (light grey

126   shades correspond to high densities and dark grey shades correspond to low densities). The system was

127   equipped with the high energy table open scanner with the 130 keV micro-focus X-ray source, flat panel

128   sensor of the large format (5 Mpx) and special protection by a lead-glass fiber-optic window (Figure 3).

129   The scanner possessed a precision object manipulator that allowed for a very precise and automatic

130   specimen   positioning.   There   were   several   filters   available   in   the   front   of   the

131   X-ray detector: 0.25 mm brass filter, 1.0 mm aluminium filter, 2.0 mm lead filter and 0.25 mm copper

132   filter. As compared to usual micro-tomography systems, it has two important advantages: a) large

133   specimens up to 200 mm in diameter may be scanned and b) the specimens may be scanned with the

134   high precision of 2-3 microns. During tests on concrete cubes, the X-ray source voltage was set on

5   130 keV, current on 61 µA and exposure time on 4000 ms. The pixel size was 34.2 µm. The X-ray

6   projections were recorded with the rotation increment of 0.2º within 360º. To reduce the noise in X-ray

7   projections, the frame averaging option was chosen to be 6 and the random movement option 10. The

8   scanning time was equal to 6 hours. All specimens were scanned using the same input parameters. In

9   order to recognize pores and cracks on micro-CT scans, a threshold procedure was carefully performed,

140 based on the density of each concrete phase. The threshold in the range 0-60 from the grey level

141 histogram 0-255 was chosen. The image reconstruction was carried out with the NRecon software. After

142 the reconstruction, the images were analyzed with the CTAn software and finally the CTVox software

143 was used to prepare the volume-rendering image reconstruction. The software programs were developed

144 by the firm Bruker mico-CT (https://www.bruker.com/products/microtomography.html).

145

146 Figure 4 presents the view on three cubic specimens $40 \times 40 \times 40$ mm^3 (called the specimens '1'-'3')

147 before fatigue tests, based on the 3D micro-CT images. The micro-CT technology clearly reveals a

148 heterogeneous 3D material meso-structure where aggregate, cement matrix, and pores are

149 distinguishable on the images of specimens. The porous interfacial transitional zones (ITZs) around

150 aggregate grains that are a very important concrete phase in inducing micro-cracks and attracting macro-

151 cracks [26, 27] are not visible in scans due to their very small dimensions. However, they may be

152 observed and measured on the concrete surface e.g. with the aid of the 2D scanning electron microscope

153 (SEM) ([22-24]). The width of FPZs may be determined on the concrete surface by means of the digital

154 image correlation (DIC) technique ([22-24]).

155

156 **Distribution of pores**

157 Figure 5 and Table 2 show the initial 3D distribution and content of pores in non-cracked concrete

158 specimens '1'-'3' (intended for fatigue tests) of Figure 4 and '0' (intended for monotonic test). The pores

159 were divided into the so-called closed and open ones. The open pores were defined as the pores that

160 spread beyond the borders of the investigated specimen and the closed pores were defined as those in

161 the specimen's interior. The initial pore volume in the specimens '1'-'3' was 1568.4 mm^3, i.e. 2.45% of

162 the specimen volume (closed pores - 1.60% and open pores - 0.85%, Figures 4a and 5a), 1760.2 mm^3,

163 i.e. 2.75% of the specimen volume (closed pores - 2.07% and open pores - 0.68%, Figures 4b and 5b)

164 and 1516.8 mm^3, i.e. 2.37% of the specimen volume (closed pores - 1.98% and open pores - 0.39, Figures

165 4c and 5c). The pores with the diameter smaller than 1.0 mm constituted about 25-30%, the pores with

166 the diameter 1.0 mm - 2.0 mm represented about 20-30% and the pores with the diameter larger than 2.0

167 mm formed about 40-50% of the total pore volume in concrete specimens. The specimen '0' that was

168 subjected to monotonic static compression had the similar initial pore volume (1817.6 mm^3) as the

169 specimens '1'-'3'.

0

3. Experimental results of fatigue compressive tests

2

3 The fatigue cyclic loading tests were carried out on 3 concrete specimens $40 \times 40 \times 40$ mm^3 with the

4 control of both the stress level and stress ratio. The continuous fatigue tests were performed for the

5

specimens '1' and '2'. For those specimens, the initial (non-cracked specimens) and final (cracked specimens) micro-CT images were only shot whereas for the specimen '3', some micro-CT scans were shot during the entire fatigue test. The specimens were always unloaded for scanning (scanning lasted each time 6 hours). Next, the compression test was continued. The scanning took place after N_i=10,000, 30,000, 60,000 and 70,000 cycles, so in total, five 3D micro-CT scanning series were performed (including initial scans before the tests). Note that unloaded periods for scanning may slightly affect fracture since some crack recovery (cracks' closure) occurred during those rest periods [38]. The number of loading cycles leading specimens to the failure (fatigue life cycles) of the specimens '1'-'3' is shown in Table 3. It was between N=71,000 and 80,000 cycles (i.e. slightly higher than that (60,000) according to [14]).

The stress-displacement diagrams σ=f(u) for the concrete specimens '1'-'3' during the cyclic fatigue tests as compared to the monotonic static test is shown in Figure 6. Figure 7 presents the zoom on the experimental vertical displacement u of the specimen '3' in cyclic uniaxial compression versus the cycle number N_i with the marked breaks for scanning. In the monotonic test, the curve σ=f(u) included obviously the elastic, hardening and softening region (Figure 6).

The external 3D micro-CT images of cubic cracked concrete specimens '1'-'3' and '0' are presented in Figure 8. The specimens '1'-'3' were scanned close to failure (Table 3) for N_i=70,000 and the observed pattern of pores including cracks is shown in Figure 9. Table 4 includes the volumes of pores and cracks in concrete specimens '1'-'3' after 70,000 cycles and in the specimen '0" after the monotonic test.

After the tests, the specimens were strongly cracked (Figures 8 and 9). The vertical cracks that propagated through the entire specimen height were predominant. There existed 6, 2 and 4 main vertical macro-cracks in the entire concrete specimens '1'-'3' (Figure 8). Moreover, in the specimens '1' and '3' some diagonal cracks can also be observed. The cracking slightly varied along the height of specimens due to the effect of boundary conditions in tests [39, 40]. The cracks were curved due to the presence of stochastically located aggregate particles. Initially, the cracking process was induced due to some stress concentrations close to the cube corners (see Figures 12 and 13) where the inclined micro-cracks appeared and coalesced. Next, some vertical cracks started to concentrate along lateral both edges and surfaces of specimens by forming column-like regions. The macro-cracks were the widest on external parts of concrete cubes at lateral edges that finally lead to concrete spalling from specimen cores [23], [41]. The concentration extent of cracking regions throughout the specimen was similar in monotonic and fatigue tests, based on the visual inspection (compare Figures 9b and 9d). However, wider macro-

209   cracks (compare Figures 9a and 9c) and more damaged aggregate particles were noticed during fatigue

210   tests.

211

212   Due to cracking, the insignificant volumetric changes of open and the pronounced changes of closed

213   pores happened during fatigue tests (Table 4, Figure 10). The crack volume was calculated as the total

214   volume of pores in the cracked specimen reduced by the total volume of pores in the initial non-cracked

215   specimen. The cracks' volume and the %-volume of open pores increased in all specimens. In contrast,

216   the %-volume of closed pores decreased in the specimens The cracks' volume increased during fatigue

217   test by 3.43%-5.62% in the specimens '1'-'3'. The %-volume of open pores increased by 1.86%-4.38%

218   and the %-volume of closed pores decreased by 0.2%-0.74%. The increase of the cracks' volume and

219   open pores in the specimen '0' (monotonic test) was smaller on average by about 30% than during

220   fatigue tests. The greatest macro-crack width in the entire specimens' volume (after unloading) was

221   w_c=0.42 mm (specimen '0'), w_c=0.61 mm (specimen '1'), w_c=0.56 mm (specimen '2') and w_c=0.72 mm

222   (specimen '3'). The pores were practically not crossed by cracks since insignificant volume changes of

223   closed pores took place (connected with strong volume changes of open pores) (Table 4).

224

225   Figure 11 shows the cross-sectional micro-CT images of the cracked specimens '1'-'3' and '0' (one

226   horizontal and two vertical in the mid-specimen that intersected the specimen centroid). They show that

227   cracks mainly propagated through the cement matrix and ITZs which were the weakest zones in concrete.

228   The micro-cracks occurred first in porous ITZs around aggregate particles and then they connected

229   themselves through a bridging mechanism ([22-24]). When two interfacial cracks happened around

230   adjacent aggregate particles, a crack inside the cement matrix bridged those interfacial cracks so that a

231   connected crack path was formed. The cracks also propagated sometimes through single weak aggregate

232   particles (Figure 12). The cracks' branching also occurred (Figure 12).

233

234   Figures 13 and 14 show the external 3D micro-CT images of the concrete specimen '3' for the different

235   cycle number N_i: N_1=0 (step "0" - initial scan), N_3=30,000 (step "2"), N_4=60,000 (step "3") and

236   N_5=70,000 (step "4"). The results for N_2=10,000 were not presented since the cracks insignificantly

237   developed. The different three cross-sectional micro-CT images of the mid-region (one horizontal and

238   two vertical that intersected the specimen centroid) for the different number of loading cycles N_i are

9   demonstrated in Figure 15.

0

1   For N_i=10,000 cycles (Figure 15B), the thin cracks occurred with the width up to w_c=0.04 mm. The

2   cracks had an irregular shape and were mainly concentrated along one vertical (lateral) edge of the

3   specimen. All micro-cracks occurred in ITZs between the cement matrix and aggregate particles and

7

244   propagated next in the cement matrix. For N_3=30,000 cycles (Figures 13b, 14b and 15C) further

245   development of existing internal cracks took place (they propagated into the depth of the cement matrix)

246   and the new macro-cracks occurred (one at the other lateral edge and one on the lateral surface). In total,

247   7 broken aggregate particles were detected in the entire specimen. The greatest crack width in the entire

248   volume was w_c=0.16 mm. After N_4=60,000 cycles (Figures 13c, 14c and 15D) the existing vertical

249   macro-cracks further evolved along lateral edges and two of those cracks propagated through the

250   specimen height. The maximum crack width was w_c=0.42 mm. The number of broken aggregate particles

251   was 13. For N_5=70,000 cycles (Figures 13d, 14d and 15E), four main vertical macro-cracks of an

252   irregular shape and a variable width might be observed (two cracks were located along two lateral edges

253   and two cracks were concentrated on the lateral surface of the specimen). The macro-cracks intersected

254   the concrete specimen. In addition, one macro-crack occurred along a horizontal edge and one inclined

255   macro-crack appeared in the upper region on the second lateral surface. The main macro-cracks were

256   connected through a network of small cracks. The largest crack width was equal to w_c=0.72 mm. The

257   number of broken aggregate particles increased up to 28. Finally, the specimen damage occurred along

258   the edge wherein the dominant vertical macro-crack was located.

259

260   Table 5 and Figures 16 and 17 present the detailed data on the volume changes of pores and cracks in

261   the concrete specimen '3' with increasing damage parameter (expressed by the quotient of the number

262   of cycles N_i and the fatigue life N=73,127, Table 3). The line connecting the measurement points was

263   approximated in Figures 16 and 17 by a polynomial function. The volume of closed pores slightly

264   decreased during the entire test (Figure 16). In the step "1", the insignificant volume changes of open

265   pores and cracks were obtained as compared to the step '0'. The maximum crack width in the entire

266   volume was w_c=0.04 mm (after the specimen unloading). In the step "2", the volume of pores and cracks

267   increased by about 50%. The greatest crack width in the entire volume was w_c=0.16 mm (after the

268   specimen unloading). In the step "3", the volume of pores and cracks increased as compared to the step

269   '2' by about 40%. The maximum crack width in the entire volume was w_c=0.42 mm (after the specimen

270   unloading). In the last step "4", the volume of pores and cracks increased as compared to the step '3' by

271   about 40%. The largest crack width in the entire volume was w_c=0.72 mm. (after the specimen

272   unloading). The increase of the cracks' volume with increasing damage parameter was strongly non-

273   linear. The relationship in Figure 17 may be divided into three parts: 1) between the damage parameter

4   0 (N_1=0) and damage parameter 0.14 (N_2=10,000) (so-called the micro-crack part), 2) between the

5   damage parameter 0.14 (N_2=10,000) and damage parameter 0.85 (N_4=60,000) (so-called the transitory

6   part) and 3) between the damage parameter 0.85 (N_4=60,000) and damage parameter ~1.0 (N_5=70,000)

7   (so-called the crack extension part [41]) (Figure 17). The damage rate was in particular strong in the last

8   fatigue stage (crack extension region) between N_4=60,000 and N_5=70,000 cycles.

8

In Figures 18 and 19, the attention is focused on the largest crack volume growth in the crack extension region before the specimen failure. The volume of cracks between those 2 different cycles' numbers increased by 2.26% (40% of the total cracks' growth) (Figure 18d, Table 5). The %-volume of closed pores decreased from 1.34% down to 1.24% (the decrease of about 10%) and the %-volume of open pores increased from 4.39% up to 6.75% (the increase of about 50%). The width of cracks, which was very non-uniformly distributed in the specimen, increased on average by 0.1-0.2 mm (Figure 18). However, in some specimen regions, it increased even by 0.3 mm.

Our experiments on concrete fatigue will be continued. An extended X-ray micro-computed tomography system will be used soon, i.e. the tomography system SkyScan 1173 will be connected to the loading machine ISTRON 5569 to make images of deforming concrete specimens during a continuous deformation process, i.e. without unloading for scanning.

4. Conclusions

This paper presents the results of experimental research work showing the 3D fracture evolution in plain concrete specimens under fatigue compression obtained by X-ray micro-CT that is a powerful tool to measure the internal damage of concrete specimens. For plain concrete under fatigue compression, the following conclusions can be offered:

- The increase of the cracks' volume with increasing damage (expressed by the quotient of the number of cycles and fatigue life) was about hyperbolical in shape. The volume of cracks close to the failure load was 3.4-5.6% of the entire specimen volume during fatigue tests. Due to cracking, the %-volume of closed pores decreased by about 30% and the %-volume of open pores increased 5-15 times. In the last loading stage between 60,000 and 70,000 cycles, the cracks' volume strongly increased (by 2.26%), i.e. almost 40% of the total crack volumetric growth.

- The growth of the total fracture volume in fatigue tests was higher by 30% as compared to the monotonic test.

- A similar crack pattern was obtained in specimens under monotonic and cyclic loading although the latter was on more damaged. The cracking pattern was strongly non-uniform. The greatest cracks' width was in the range of 0.56-0.72 mm (fatigue tests) and 0.42 mm (monotonic test). The cracks that initially occurred in ITZs and propagated through the cement matrix by bridging, were strongly curved. However,

several cracks also propagated through weak aggregate particles. At the failure, the lateral sides of specimens separated from the cores.

References

[1] Aas-Jakobsen K. Fatigue of concrete beams and columns. *Institute for Betonkonstruktioner Bulletin* 1970; 70(1).

[2] Tepfers R, Kutti T. Fatigue strength of plain and ordinary and lightweight concrete. *ACI Journal*, 1979; 76(5): 635-652.

[3] Hsu TCT. Fatigue of plain concrete. *Journal of the American Concrete Institute* 1981;78(8): 292-305.

[4] Petkovic G, Lenschow R, Stemland H, Rosseland S. Fatigue of high-strength concrete, *ACI SP-121: High-strength concrete* 1990 505-525.

[5] Kim, JL, Kim YY. Experimental study of the fatigue behavior of high strength concrete, *Cement and Concrete Research* 1996;26(10):1513-1523.

[6] Tue NV, Mucha S. Fatigue behaviour of high strength concrete under compression, *Bautechni*k 2006;83(7):497-504 (in German).

[7] Lohaus L, Wefer M, Oneschkow N, Design model for the fatigue behaviour of normal strength, high strength and ultra-high strength concrete. *Beton- und Stahlbetonbau* 2011; 106(12):836–846. (in German).

[8] Jiang C, Gu X, Huang Q. Zhang W. Deformation of concrete under high-cycle fatigue loads in uniaxial and eccentric compression. *Construction and Building Materials* 2017;141:379-39.

[9] Lu J, Zhu K, Tian L, Guo L. Dynamic compressive strength of concrete damaged by fatigue loading and freeze-thaw cycling, *Construction and Building Materials* 2017; 15:847-855.

[10] Fan J, Jiang D, Chen J, Liu W, Ngaha WT, Chen J. Fatigue performance of ordinary concrete under discontinuous cyclic loading. *Construction and Building Materials* 2018; 166:974-981.

[11] Liang J, Ding Z, Li J. A probabilistic analyzed method for concrete fatigue life, *Probabilistic Engineering Mechanics* 2017;49:13-21.

[12] Shi XP, Fwa TF, Tan SA. Flexural fatigue strength of plain concrete, *ACI Materials Journal* 1993;90(5):435-440.

[13] Lantsoght E, van der Veen C, de Boer A, Proposal for the fatigue strength of concrete under cycles of compression. *Construction and Building M*aterials 2016;107:138-156.

[14] Model Code 2010. Final draft. FIB Bulletin, EPFL Lausanne 2012.

[15] Eurocode 2 Design of concrete structures. European Committee for Standardization. EN 1992-2:2005/AC:2008. Brussels (Belgium): European Standards 2008.

[16] ACI 215R-74 Considerations for design of concrete structures subjected to fatigue loading. *ACI Committee 215,* 1997; 71(3), 97-121.

[17] Ceb Committee GTG 15. Fatigue of concrete structures. CEB Bulletin d'information, No 188, Lausanne, Switzerland: European Concrete Committee, 1988.

[18] Balázs GL, Fatigue of bond, *ACI Materials Journal* 1991; 88(6):620-629.

[19] Vicente MA, Ruiz G, Gonzalez DC, Minguez J, Tarifa JM, Zhang XX. CT-Scan study of crack patterns of fiber-reinforced concrete loaded monotonically and under low-cycle fatigue, *International Journal of Fatigue* 2018; 114:138-147.

[20] Skarżyński L, Tejchman J. Experimental investigations of fracture process in concrete by means of X-ray micro-computed tomography. *Strain* 2016;52:26-45.

[21] Vicente MA, Mínguez J, González DC, Book chapter: the use of computed tomography explore the microstructure of materials in civil engineering: from rocks to concrete (in: Halefoglu A.M., editor) *Computed tomography - advanced applications*. InTech, 2017, pp. 207-230.)

[22] Skarżyński L, Nitka M, Tejchman J. Modelling of concrete fracture at aggregate level using FEM and DEM based on X-ray μCT images of internal structure. *Engineering Fracture Mechanics* 2015; 147:13-35.

[23] Suchorzewski J, Tejchman J, Nitka M. DEM simulations of fracture in concrete under uniaxial compression based on its real internal structure. *Int. J. Damage Mechanics 2018;*27(4):578-607.

[24] Suchorzewski J, Tejchman J, Nitka M, Experimental and numerical investigations of concrete behaviour at meso-level during quasi-static splitting tension. *Theoretical and Applied Fracture Mechanics* 2018;96:720-739.

[25] Skarżyński L, Suchorzewski J. Mechanical and fracture properties of concrete reinforced with recycled and industrial steel fibers using Digital Image Correlation technique and X-ray micro-computed tomography. *Construction and Building Materials* 2018;183:283-299.

[26] Nitka M,. Tejchman J. A three-dimensional meso-scale approach to concrete fracture based on combined DEM with X-ray μCT images. *Cement and Concrete Research* 2018;107:11-29.

[27] Suchorzewski J, Tejchman J, Nitka M, Bobiński J. Meso-scale analyses of size effect in brittle materials using DEM. *Granular Matter* 2018 (in review).

[28] Trawinski, W., Bobinski, J. and Tejchman, J. Two-dimensional simulations of concrete fracture at aggregate level with cohesive elements based on X-ray micro-CT images. *Engineering Fracture Mechanics* 2016; 168: 201-226.

[29] Trawiński W, Tejchman J, Bobiński J. A three-dimensional meso-scale approach with cohesive elements to concrete fracture based on X-ray μCT images. *Engineering Fracture Mechanics* 2018;189: 27-50.

[30] Ray S, Kishen JMC. Fatigue crack propagation model for plain concrete–An analogy with population growth, *Engineering Fracture Mechanics* 2010;77:3418–3433.

[31] Simon KM, Kishen, J.M.C. A multiscale approach for modeling fatigue crack growth in concrete. *International Journal of Fatigue* 2017;98 :1-13.

[32] Chaboche JL, Lesne PM. A nonlinear continuous fatigue damage model. *Fatigue & Fracture Engineering Materials & Structures* 1998 ;11:1-17.

[33] Papa, E, Taliercio A. Anisotropic damage model for the multiaxial static and fatigue behaviour of plain concrete. *Engineering Fracture Mechanics* 1996;55:163-179.

[34] Alliche, A. Damage model for fatigue loading of concrete. *International Journal of Fatigue* 2004;26:915-921

[35] Nguyen NHT, Buia HH, Kodikara J, Aroorana S, Darve F. A discrete element modelling approach for fatigue damage growth in cemented materials. *International Journal of Plasticity* 2018, https://doi.org/10.1016/j.ijplas.2018.08.007.

[36] Wagner P, Schwarzhaupt O, May M. In-situ X-ray computed tomography of composites subjected to fatigue loading. *Materials Letters* 2019;236:128-130.

[37] Harimon, MA, Miyashita *Y*, Yuichi Otsuka Y, Mutoh Y, Yamamoto, *S*. High temperature fatigue characteristics of P/M and hot-forged W-Re and TZM for X-ray target of CT scanner. *Materials & Design* 218;137:335-344.

[38] Hilsdorf, HK, Kesler CE. Fatigue Strength of Concrete Under Varying Flexural Stresses. *Proc. American Concrete Institute* 1966; 63:1059-1075.

[39] van Vliet, MRA, van Mier JGM. Experimental investigation of concrete fracture under uniaxial compression. *Mechanics of Cohesive-Frictional Materials* 1996;1:115–127.

[40] del Viso, JR, Carmona, JR, Ruiz G. Shape and size effects on the compressive strength of high-strength concrete, *Cement and Concrete Research* 2008;38:386-395.

[41] Li Q, Huang H, Xu S, Zhou B, Yu RC. Compressive fatigue damage and failure mechanism of fiber reinforced cementitious material with high ductility. *Cement and Concrete Research* 2016;90:174-183.

LIST OF FIGURES

Figure 1: Particle size distribution curve of concrete (maximum diameter d_{max}=16 mm and mean diameter d_{50}=2 mm)

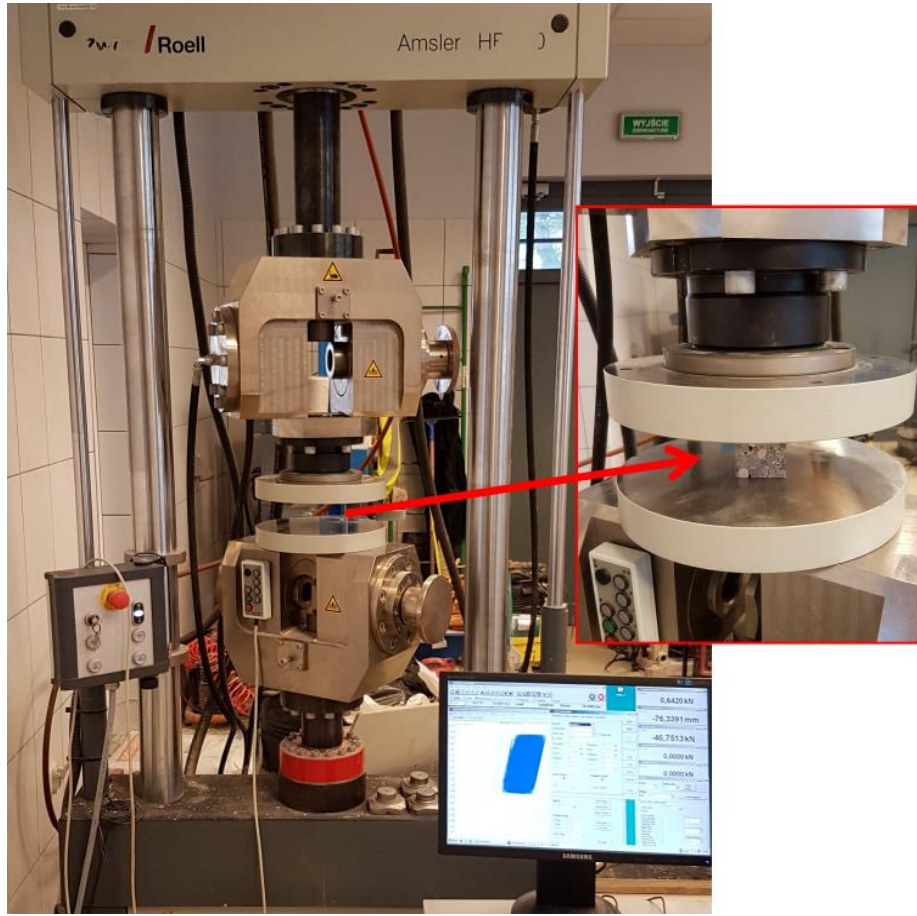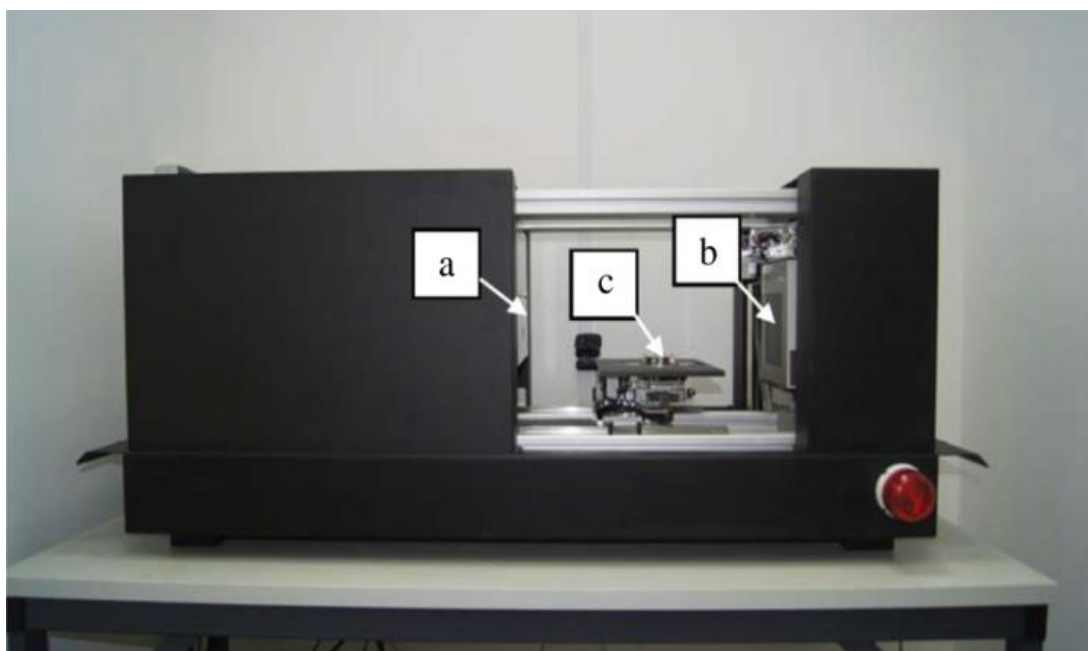**Figure 2:** Testing servo-hydraulic machine Zwick Roell HB250 with the concrete specimen for fatigue tests (marked with the arrow)

Figure 3: X-ray micro-tomography station SkyScan 1173 [20]: a) X-ray source, b) flat panel and c) precision object manipulator

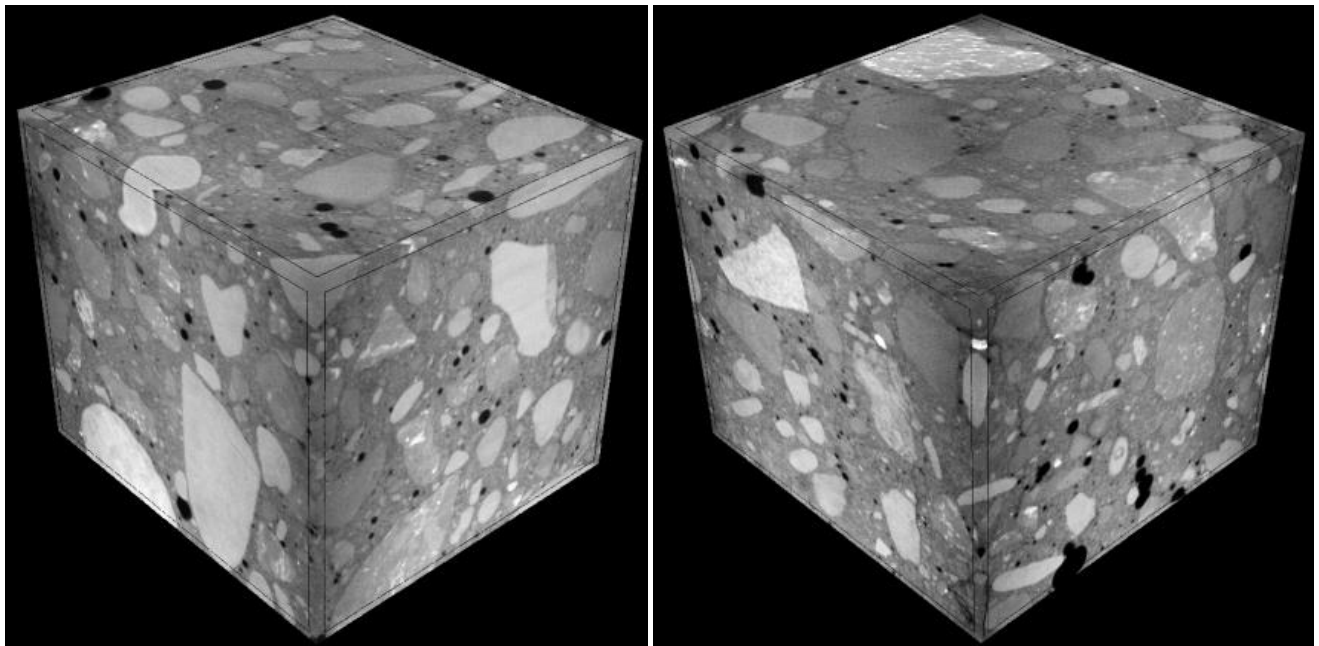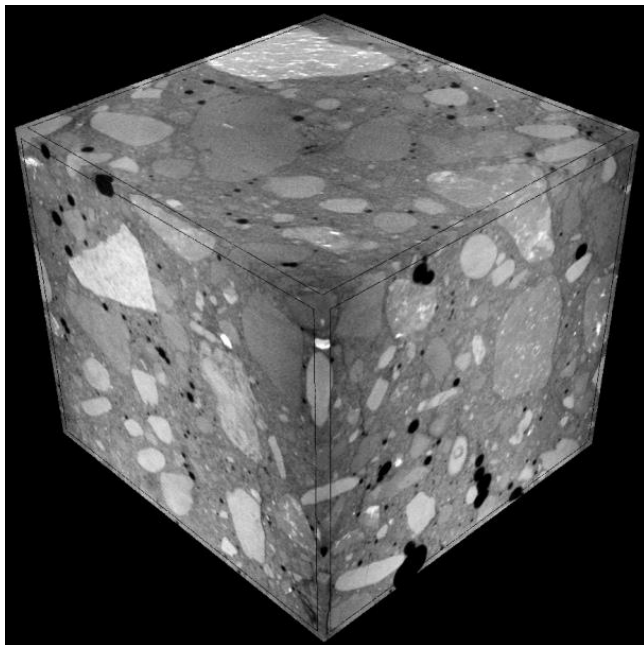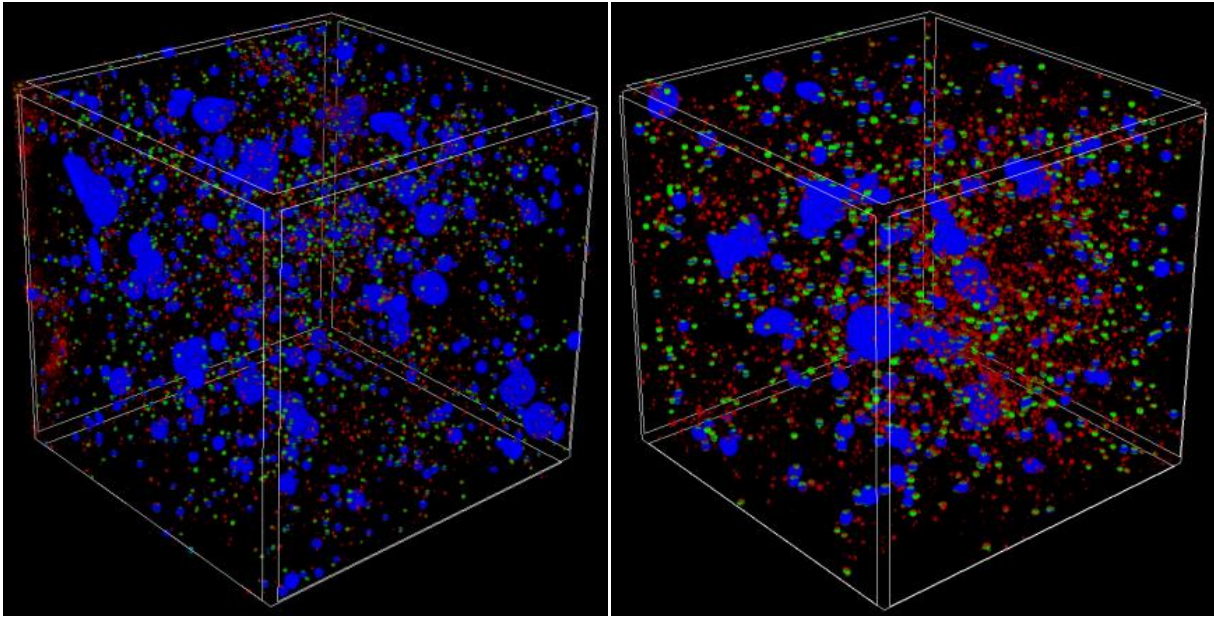**Figure 4**: Initial 3D external X-ray micro-CT images of cubic concrete specimens before fatigue tests: a) specimen '1', b) specimen '2' and c) specimen '3' (black colour denotes pores)

Figure 5: Initial diameter distribution of pores inside of non-cracked concrete specimens of Figure 4 before fatigue tests: a) specimen '1', b) specimen '2' and c) specimen '3' (colours denote diameter in range of ≤1.0 mm (red colour), 1.01 mm - 2.0 mm (green colour) and ≥2.0 mm (blue colour))

Figure 6: Experimental vertical normal stress σ versus vertical displacement u from monotonic and cyclic uniaxial compression tests (a) quasi-static test, b) fatigue test '1', c) fatigue test '2' and d) fatigue test '3')

Figure 7: Experimental vertical displacement u from cyclic uniaxial compression tests versus the number of cycles N for concrete specimen '3' (vertical dashed lines denote breaks for X-ray micro-CT scanning)

Figure 8: External 3D X-ray micro-CT images of cracked cubic concrete specimens close to failure during cyclic and monotonic tests in compression: a) specimen '1', b) specimen '2', c) specimen '3' in cyclic tests and d) specimen '0' in monotonic test (black colour denotes both pores and cracks)

Figure 9: Internal 3D micro-CT images of pores and cracks in cubic concrete specimens close to failure during cyclic and monotonic tests: a) specimen '1'b) specimen '2', c) specimen '3' in cyclic tests and d) specimen '0' in monotonic test (colours denote macro-pores' diameter in range of ≤1.0 mm (red colour), 1.01 mm - 2.0 mm (green colour) and ≥2.0 mm (blue colour))

13

452

Figure 10: Volume changes of pores and cracks in concrete specimens '0'-'3' during uniaxial fatigue compression: a) volume of closed pores, b) volume of open pores and c) volume of cracks (× - initial value before test and ● - final value after test)

Figure 11: 2D micro-CT images of cracked cubic specimens close to failure: A) specimen '1', B) specimen '2', C) specimen '3' (fatigue tests) and D) specimen '0' (monotonic test) (a) and b) two vertical mid-specimen cross-sections and c) horizontal mid-specimen cross-section, black colour denotes pores and cracks)

Figure 12: View on crack branching and crack propagating through weak aggregate particle

Figure 13: Cracking evolution in cubic concrete specimen '3' from 3D micro-CT images in fatigue tests: a) before test (Figure 4c), b) after N_3=30,000 cycles c) after N_4=60,000 cycles and d) after N_5=70,000 cycles

Figure 14: Evolution of pores and cracks in cubic concrete specimen '3' from 3D micro-CT images in fatigue tests: a) before test (Figure 5c), b) after 30,000 loading cycles c) after 60,000 loading cycles and d) after 70,000 loading cycles colours denote pores' diameter in range of ≤1.0 mm (red colour), 1.01 mm - 2.0 mm (green colour) and ≥2.0 mm (blue colour))
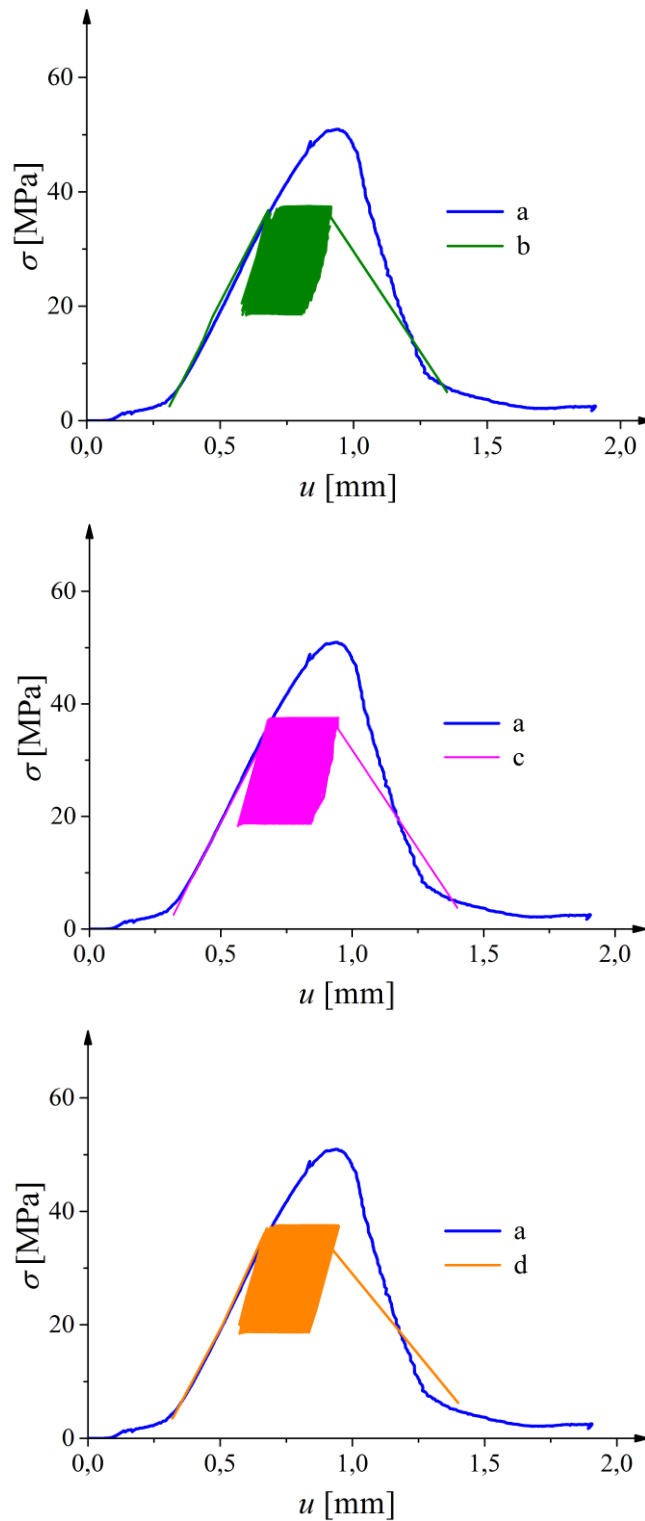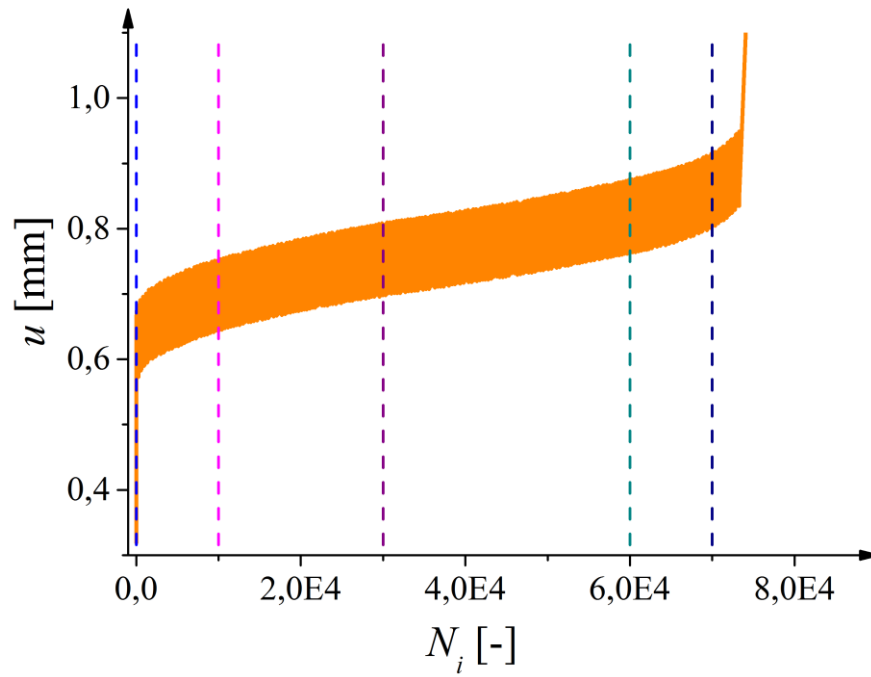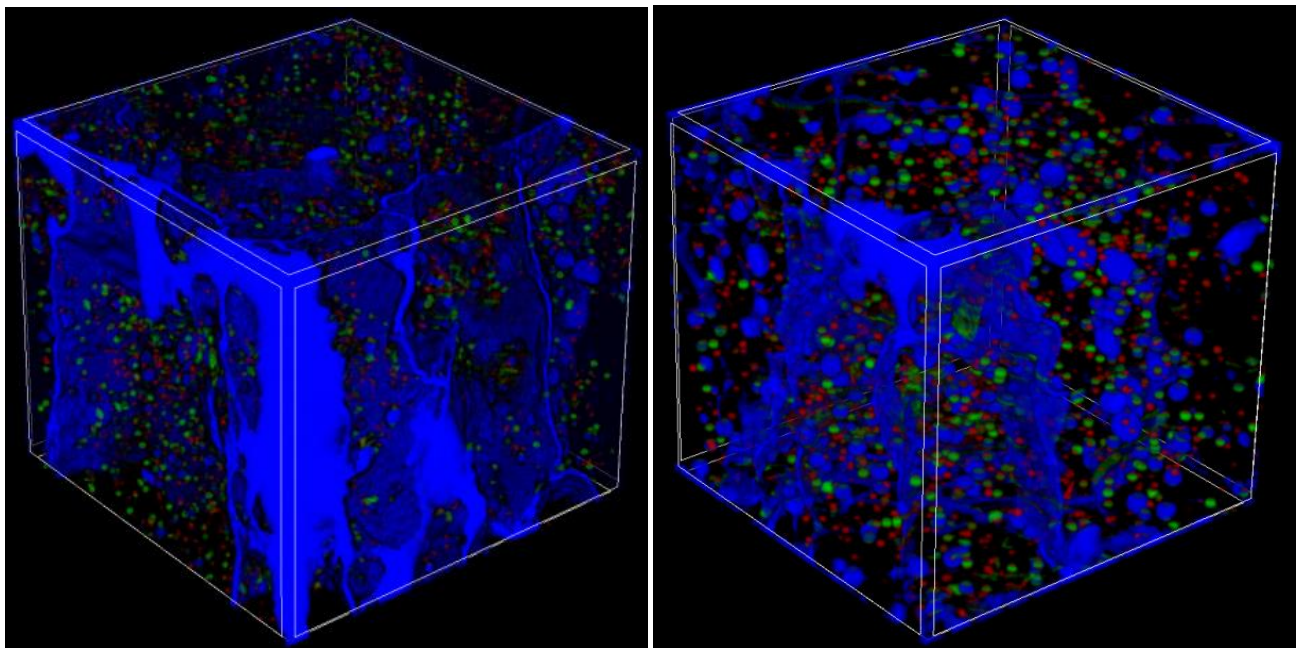
Figure 15: 2D micro-CT images of cracked cubic specimen '3' for different deformation steps: A) step "0", B) step 1", C) step "2", D) step "3" and E) step "4" (a) and b) two vertical mid-specimen cross-sections and c) horizontal mid-specimen cross-section, black colour denotes pores and macro-cracks)

Figure 16: Evolution of volume of closed pores (a) and open pores (b) with increasing damage (expressed by quotient of number of loading cycles N_i and fatigue life N) in concrete specimen '3'

Figure 17: Evolution of crack volume V versus damage (expressed by quotient of number of loading cycles N_i and fatigue life N) in concrete specimen '3'

Figure 18: Distribution of pores and cracks in specimen '3': a) non-cracked concrete specimen (white colour), b) after N_4=60,000 cycles (green colour), c) after N_5=70,000 loading cycles (green and red colour) and d) between N_4=60,000 and N_5=70,000 cycles (red colour)

14

487   **Figure 19**: Micro-CT image of distribution of crack width's growth between N_4=60,000 and N_5=70,000

488   cycles in concrete specimen '3' of Figure 18d

489

490
491
492
493
494
495
496
497
498
499
500
501
502
503
504
505
506
507
508
509
510
511
512
513
514
515
516
517
518
519
520
521
522
523
524
525
526
527
528
529
0
1
2
3
4
5
6

15

LIST OF FIGURES

537
538
539
540
541

542
543
544
545

Figure 1: Particle size distribution curve of concrete (maximum diameter d_{max}=16 mm and mean diameter d_{50}=2 mm)

FIGURE 1

553
554
555

556
557

558 **Figure 2:** Testing servo-hydraulic machine Zwick Roell HB250 with concrete specimen for the fatigue
559 tests (marked with the arrow)

560
561

562 **FIGURE 2**

563
564
565
6
7

568

569

570

571

Figure 3: X-ray micro-tomography station SkyScan 1173 [20]: a) X-ray source, b) flat panel and
c) precision object manipulator

574

575

576

577   **FIGURE 3**

578

579

580

581

582

583

584

585   a)   b)

586   c)

587

Figure 4: Initial 3D external X-ray micro-CT images of cubic concrete specimens before fatigue tests:

a) specimen '1', b) specimen '2' and c) specimen '3' (black colour denotes pores)

FIGURE 4

593

594
595   a)   b)

596   c)
597

Figure 5: Initial diameter distribution of pores inside of non-cracked concrete specimens of Figure 4 before fatigue tests: a) specimen '1', b) specimen '2' and c) specimen '3' (colours denote diameter in range of ≤1.0 mm (red colour), 1.01 mm - 2.0 mm (green colour) and ≥2.0 mm (blue colour))

601

FIGURE 5

2

3

Figure 6: Experimental vertical normal stress σ versus vertical displacement u from monotonic and cyclic uniaxial compression tests (a) quasi-static test, b) fatigue test '1', c) fatigue test '2' and d) fatigue test '3')

FIGURE 6

21

605
606
607
608 **Figure 7**: Experimental vertical displacement u from cyclic uniaxial compression tests versus the
609 number of cycles N_i for concrete specimen '3' (vertical dashed lines denote breaks for X-ray micro-CT
610 scanning)
611
612
613
614
5
6
7
8

FIGURE 7

621
622 a) b)

623
624 c) d)
625

626 **Figure 8**: External 3D X-ray micro-CT images of cracked cubic concrete specimens close to failure
7 during cyclic and monotonic tests in compression: a) specimen '1', b) specimen '2', c) specimen '3' in
8 cyclic tests and d) specimen '0' in monotonic test (black colour denotes both pores and cracks)
9

0 **FIGURE 8**

1

23

a)   b)

c)   d)

Figure 9: Internal 3D micro-CT images of pores and cracks in cubic concrete specimens close to failure during cyclic and monotonic tests: a) specimen '1'b) specimen '2', c) specimen '3' in cyclic tests and d) specimen '0' in monotonic test (colours denote macro-pores' diameter in range of ≤1.0 mm (red colour), 1.01 mm - 2.0 mm (green colour) and ≥2.0 mm (blue colour))

FIGURE 9

24

a)

b)

c)

Figure 10: Volume changes of pores and cracks in concrete specimens '0'-'3' during uniaxial fatigue compression: a) volume of closed pores, b) volume of open pores and c) volume of cracks (× - initial value before test and ● - final value after test)

FIGURE 10

653

654

655

A)

656

657

B)

658

659

C)

26

D)

a)   b)   c)

Figure 11: 2D micro-CT images of cracked cubic specimens close to failure: A) specimen '1', B) specimen '2', C) specimen '3' (fatigue tests) and D) specimen '0' (monotonic test) (a) and b) two vertical mid-specimen cross-sections and c) horizontal mid-specimen cross-section, black colour denotes pores and cracks)

FIGURE 11

679
680
681
682
683

684
685

Figure 12: View on crack branching and crack propagating through weak aggregate particle

687
688
689
690

FIGURE 12

692

693

694

695
a)   b)

696
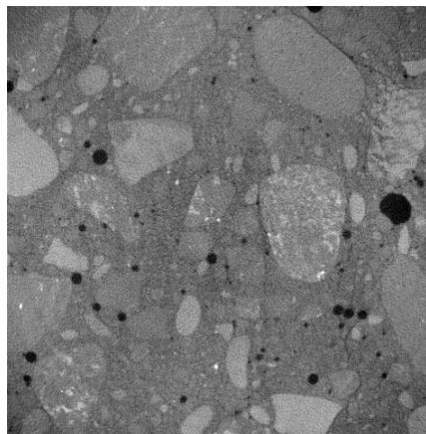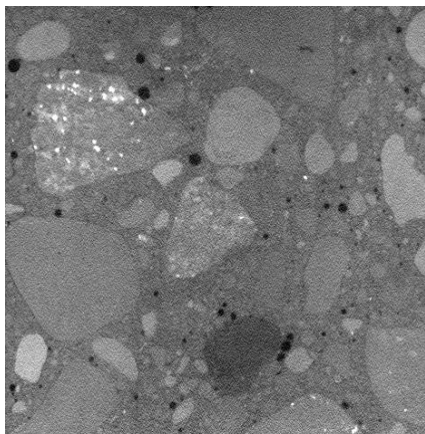
697
c)   d)

698

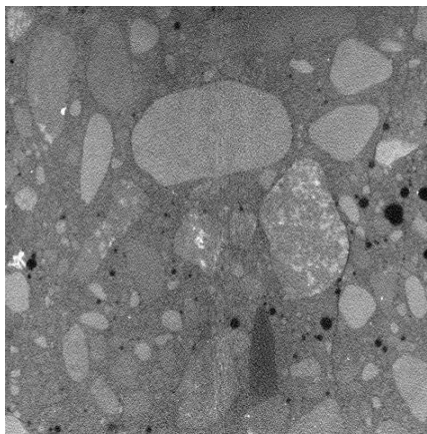699   **Figure 13**: Cracking evolution in cubic concrete specimen '3' from 3D micro-CT images in fatigue tests:

700   a) before test (Figure 4c), b) after N_3=30,000 cycles c) after N_4=60,000 cycles and d) after N_5=70,000

1   cycles

2

3   **FIGURE 13**

4

706

707
a)   b)

708
709
c)   d)

Figure 14: Evolution of pores and cracks in cubic concrete specimen '3' from 3D micro-CT images in fatigue tests: a) before test (Figure 5c), b) after 30,000 loading cycles c) after 60,000 loading cycles and d) after 70,000 loading cycles (colours denote pores' diameter in range of ≤1.0 mm (red colour), 1.01 mm - 2.0 mm (green colour) and ≥2.0 mm (blue colour))
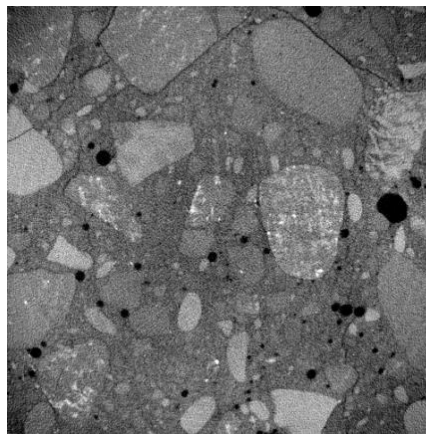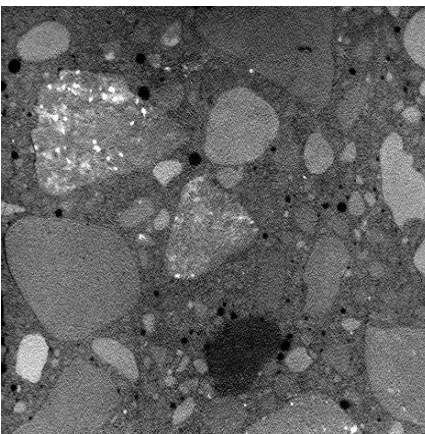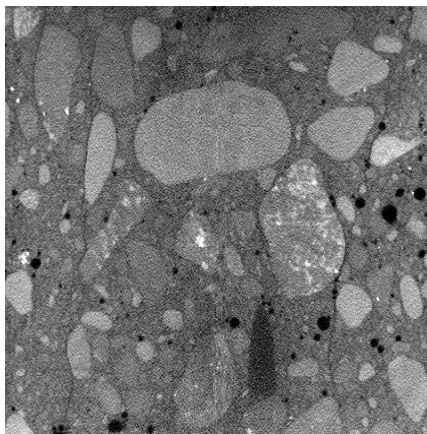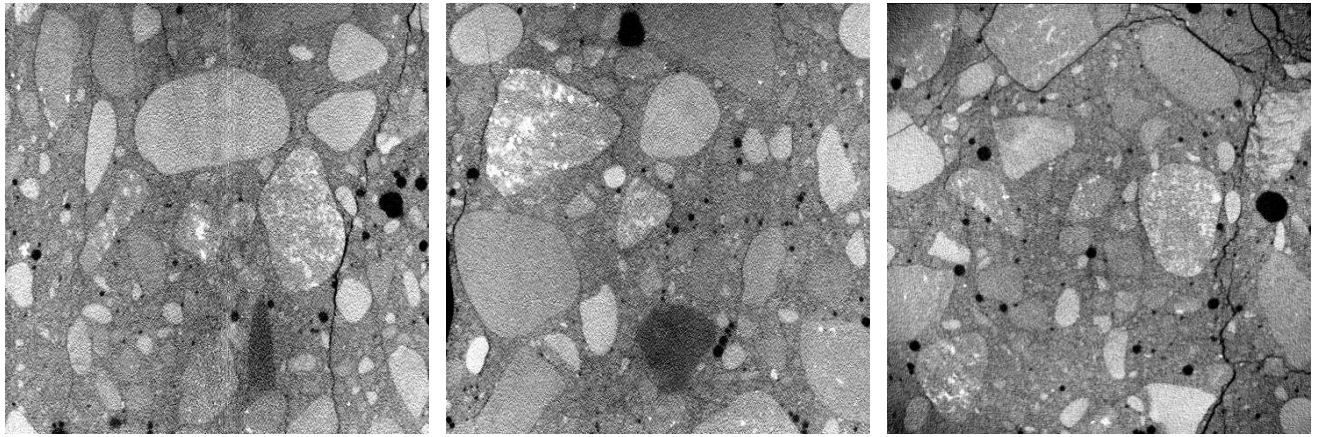
FIGURE 14

A)

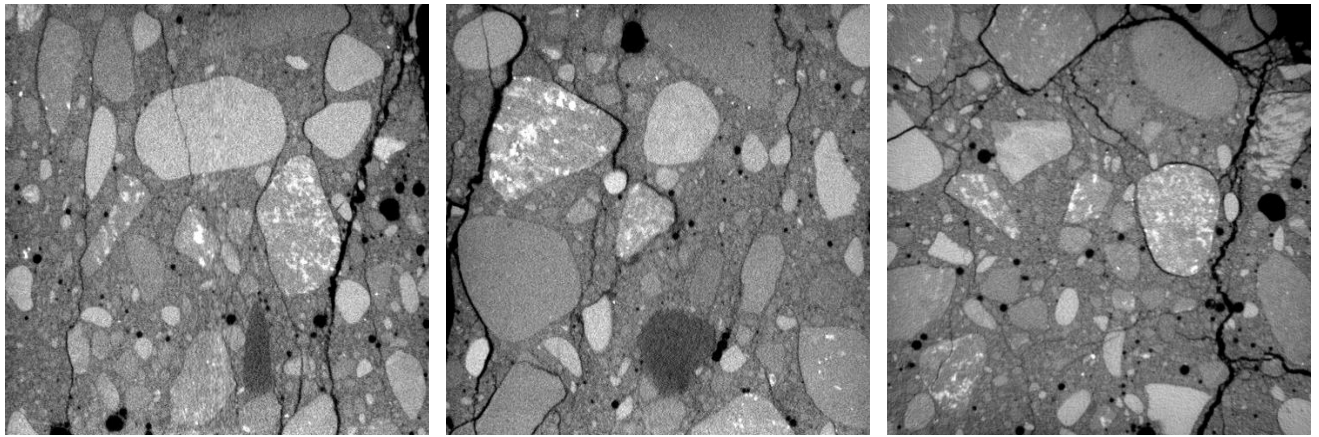B)

C)

D)

E)

a)   b)   c)

Figure 15: 2D micro-CT images of cracked cubic specimen '3' for different deformation steps: A) step "0", B) step 1", C) step "2", D) step "3" and E) step "4" (a) and b) two vertical mid-specimen cross-sections and c) horizontal mid-specimen cross-section, black colour denotes pores and macro-cracks)

FIGURE 15

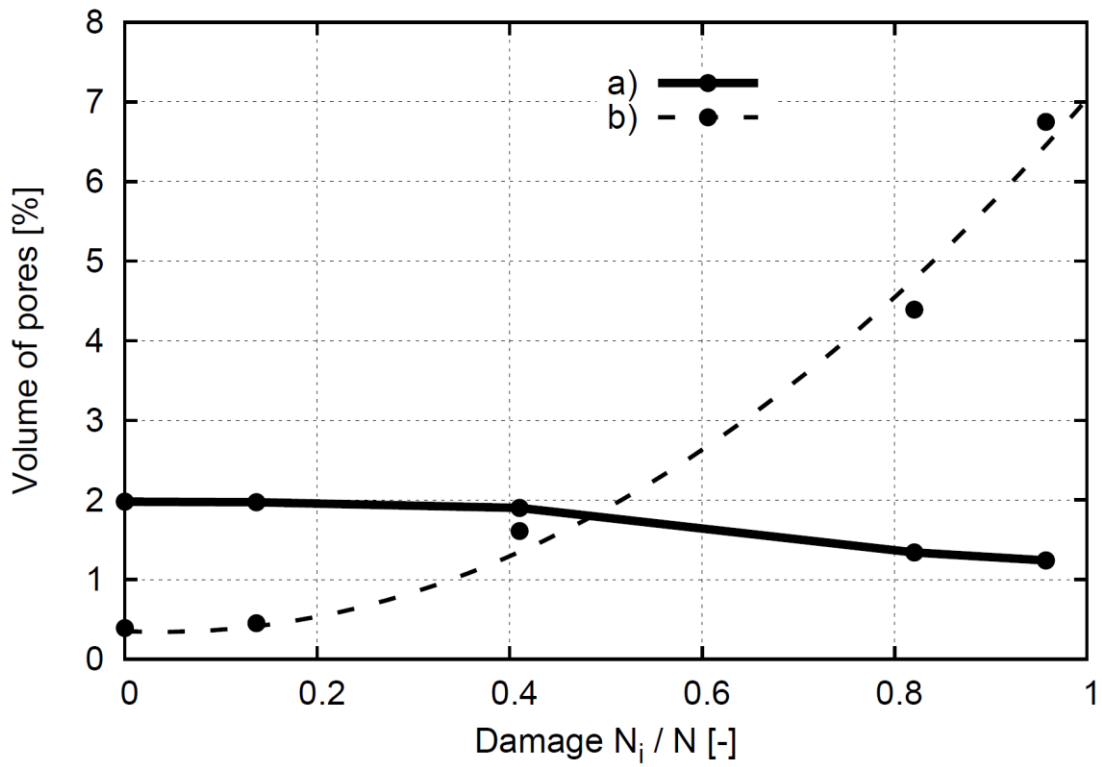32

Figure 16: Evolution of volume of closed pores (a) and open pores (b) with increasing damage

734 (expressed by quotient of number of loading cycles N_i and fatigue life N) in concrete specimen '3'

735

736

737

FIGURE 16

739

740
741
742
743
744
745

Figure 17: Evolution of crack volume *V* versus damage (expressed by quotient of number of loading cycles N_i and fatigue life *N*) in concrete specimen '3'

FIGURE 17

760
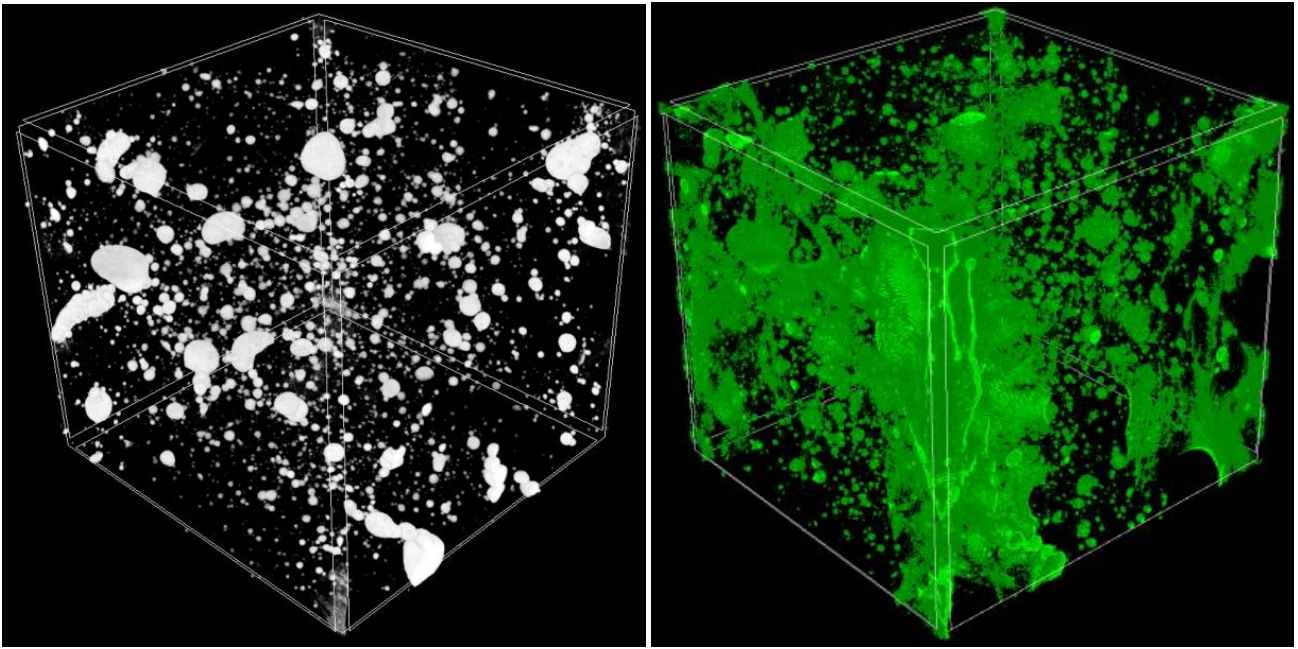
761
a)   b)

762

763
c)   d)

764

Figure 18: Distribution of pores and cracks in specimen '3': a) non-cracked concrete specimen (white colour), b) after N_4=60,000 cycles (green colour), c) after N_5=70,000 loading cycles (green and red colour) and d) between N_4=60,000 and N_5=70,000 cycles (red colour)

FIGURE 18

771
772
773
774
775

776
777
778
779
780

Figure 19: Micro-CT image of distribution of crack width's growth between N_4=60,000 and N_5=70,000 cycles in concrete specimen '3' of Figure 18d

FIGURE 19

LIST OF TABLES

Table 1: Concrete mixing composition in experiments (d_{50} – mean particle diameter, $d_{\max}$ – maximum particle diameter and β – total particle volume)

Concrete component	Content of concrete components (d_{50}=2 mm, d_{max}=16 mm, β=75%)
cement (Portland 32.5R)	810 [kg/m^3]
sand (diameter size 0-2 mm)	650 [kg/m^3]
gravel (diameter size 2-8 mm)	580 [kg/m^3]
gravel (diameter size 8-16 mm)	580 [kg/m^3]
water	340 [l/m^3]

800

801 **Table 2**: Volume and diameter range of macro-pores in initial non-cracked concrete specimens

802 (specimens '1'-'3' are presented in Figure 4)

803

Specimen number and test type	Diameter range of pores [%]				Volume of pores [mm³]	% - volume of pores [%]	% - volume of closed pores [%]	% - volume of open pores [%]
	≤0.50 mm	0.51-1.00 mm	1.01-2.00 mm	≥2.01 mm				
'0" monotonic test	12.2	11.9	28.5	47.4	1817.6	2.84	2.11	0.73
'1' fatigue test	10.2	15.4	30.5	43.9	1568.4	2.45	1.60	0.85
'2' fatigue test	14.5	16.4	22.2	46.9	1760.2	2.75	2.07	0.68
'3' fatigue test	9.8	14.1	24.5	51.6	1516.8	2.37	1.98	0.39

804

805

806

807 **Table 3:** Fatigue life results (maximum number of loading cycles leading to specimen failure) for

808 concrete specimens '1'-'3' during uniaxial compression (σ_{max} - maximum normal stress, σ_{min} - minimum

809 normal stress and f_c - uniaxial compressive strength)

810

Concrete specimen	σ_{max}/f_c	σ_{min}/f_c	Number of fatigue life cycles
'1'			71,518
'2'	0.75	0.37	80,069
'3'			73,127

1

2

38

813 **Table 4**: Volume of pores and cracks in concrete specimens '1'-'3' after 70,000 cycles and in concrete
814 specimen '0' after monotonic loading close to failure

815

Specimen number and test type	Volume of pores and cracks [mm³]	% - volume of pores and cracks [%]	% - volume of closed pores and cracks [%]	% - volume of open pores and cracks [%]	Volume of cracks [mm³]	% - volume of cracks [%]
'0' monotonic test	3750.4	5.86	1.60	4.26	1932.8	3.02
'1' fatigue test	4390.4	6.86	1.40	5.46	2822.0	4.41
'2' fatigue test	3948.8	6.17	1.56	4.61	2188.6	3.43
'3' fatigue test	5113.6	7.99	1.24	6.75	3596.8	5.62

816

817

818

819 **Table 5**: Volume of pores and cracks in concrete specimen '3' for different steps related to numbers of
820 cycles N_i

821

Step	Number of cycles N_i	Volume of pores and cracks [mm³]	% - volume of pores and cracks [%]	% - volume of closed pores and cracks [%]	% - volume of open pores [%]	Volume of cracks [mm³]	% - volume of cracks [%]
'1'	0	1516.8	2.37	1.98	0.39	0	0
'2'	10,000	1548.8	2.42	1.97	0.45	32.0	0.05
'3'	30,000	2240.0	3.50	1.90	1.61	723.2	1.13
'4'	60,000	3667.2	5.73	1.34	4.39	2150.4	3.36
'5'	70,000	5113.6	7.99	1.24	6.75	3596.8	5.62

2

3